ISSN 1063-7834, Physics of the Solid State, 2008, Vol. 50, No. 1, pp. 63–70. © Pleiades Publishing, Ltd., 2008.
Original Russian Text © V.S. Zakhvalinskiĭ, R. Laiho, T.S. Orlova, A.V. Khokhulin, 2008, published in Fizika Tverdogo Tela, 2008, Vol. 50, No. 1, pp. 61–68.

MAGNETISM AND FERROELECTRICITY

Electrical Conductivity and Magnetic Properties of $La_{1-x}Ca_xMn_{1-y}Fe_yO_3$ Ceramic Samples ($x = 0.67$, $y = 0$, 0.05)

V. S. Zakhvalinskiĭ[a], R. Laiho[b], T. S. Orlova[c], and A. V. Khokhulin[a]

[a] *Belgorod State University, ul. Pobedy 85, Belgorod, 308015 Russia*
e-mail: v_zakhval@rambler.ru, zakhvalinskii@bsu.edu.ru
[b] *Wihuri Physical Laboratory, University of Turku, Turku, FIN-20014 Finland*
[c] *Ioffe Physicotechnical Institute, Russian Academy of Sciences, Politekhnicheskaya ul. 26, St. Petersburg, 194021 Russia*

Received December 5, 2006; in final form, May 14, 2007

Abstract—The temperature dependences of the magnetic susceptibility $\chi(T)$ and the electrical resistivity $\rho(T)$ of ceramic samples of $La_{1-x}Ca_xMnO_3$ with $x = 0.67$ (LCMO) and $La_{1-x}Ca_xMn_{1-y}Fe_yO_3$ with $x = 0.67$ and $y = 0.05$ (LCMFO) are investigated in magnetic fields $B = 50$–10^5 G and the temperature range $T = 4.2$–400 K. Both samples undergo a transition from the paramagnetic state to a state with charge (orbital) ordering (CO) at temperatures $T_{CO} \approx 272$ K for LCMO and $T_{CO} \approx 222$ K for LCMFO. The behavior of the paramagnetic phase in the temperature range 320–400 K for LCMO and 260–400 K for LCMFO is described by the Curie–Weiss law with effective Bohr magneton numbers $p_{eff} = 4.83\ \mu_B$ (LCMO) and $4.77\ \mu_B$ (LCMFO), respectively. The disagreement between the observed positive Weiss temperatures ($\theta \approx 175$ K (LCMO) and $\theta \approx 134$ K (LCMFO)) and negative Weiss temperatures required for the antiferromagnetic ground state can be explained by the phase separation and transition to the charge-ordered state. The magnetic irreversibility for $T < T_{CO}$ is accounted for by the existence of a mixture of the ferromagnetic and antiferromagnetic phases, as well as the cluster glass phase. At low temperatures, doping with iron enhances the frustration of the system, which manifests itself in a more regular behavior of the decay rate of the remanent magnetization with time. The temperature dependence of the electrical resistivity in the range of the charge-ordered phase conforms to the variable-range hopping model. The behavior of the electrical resistivity is governed by the complex structure of the density of localized states near the Fermi level, which includes a soft Coulomb gap $\Delta = 0.464$ eV for LCMO and 0.446 eV for LCMFO. It is established that the ratio between the localization radii of charge carriers a for LCMFO and a_{und} for LCMO is $a/a_{und} = 0.88$.

PACS numbers: 75.47.Lx, 74.25.Fy, 74.62.Dh

DOI: 10.1134/S1063783408010137

1. INTRODUCTION

The $La_{1-x}Ca_xMnO_3$ system has a rich phase diagram [1, 2], which includes paramagnetism, ferromagnetism, antiferromagnetism, and charge and orbital ordering depending on the temperature and doping level x. The compositions at the limits of the diagram $x = 0$ and 1 are antiferromagnetic insulators of the A and G types, respectively [2], and the material with intermediate compositions is either a ferromagnetic metal ($0.15 < x < 0.50$) or a charge-ordered (CO) antiferromagnet. In compositions with $x > 0.5$, the ratio between the ferromagnetic and charge-ordered antiferromagnetic phases varies depending on the temperature. Studies of the magnetic and relaxation properties [3, 4] suggest that the two phases coexist. Several explanations were advanced in the literature to account for this behavior. On the one hand, the coexistence of phases is attributed to electronic phase separation observed in the manganites [5], while, on the other hand, phase separation is ascribed to structural inhomogeneities in ceramic samples which mediate local magnetic properties. Neutron scattering experiments suggest that the charge-ordered antiferromagnetic state may be considered a manifestation of two interpenetrating lattices of the Mn^{3+} and Mn^{4+} ions [6].

Replacement of even a small number of atoms in position B in the perovskite manganite ABO_3 structure by another transition metal affects the charge-ordering and double exchange mechanisms [7, 8]. Iron enters into the perovskite manganite structure in the form of the Fe^{3+} ion [9–11], which is close in size to Mn^{3+} [12]. The properties of $La_{1-x}Ca_xMn_{1-y}Fe_yO_3$, such as the temperature and magnetic field dependences of the electrical resistivity, magnetothermopower, and magnetization, for compositions $x < 0.5$ are presently known to a fairly good extent [9, 13–15]. The properties and fine details in the magnetic phase diagram of $La_{1-x}Ca_xMn_{1-y}Fe_yO_3$ for compositions with $x > 0.5$

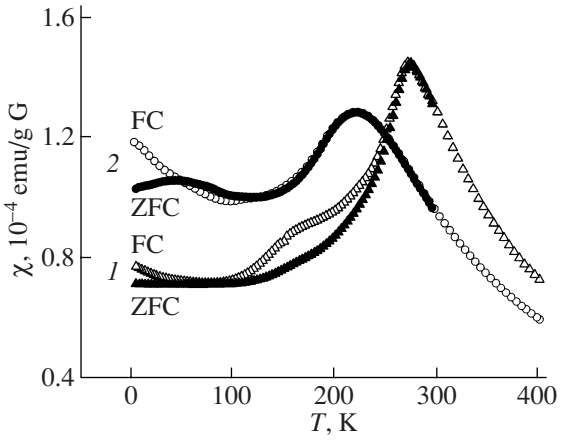

Fig. 1. Temperature dependences of the magnetic susceptibility $\chi(T)$ of the (*1*) LCMO and (*2*) LCMFO samples under FC and ZFC conditions in an external magnetic field $B = 1$ T.

have not thus far been studied to a good enough measure. Studies of charge ordering in the $La_{1-x}Ca_xMn_{1-y}Fe_yO_3$ system for $x = 0.67$ and $0 \le y \le 0.06$ were reported in [16, 17]. It was shown that the charge ordering temperature T_{CO}, just as the Curie–Weiss temperature, falls off linearly with increasing iron doping y. Direct transmission electron microscopy observation identified the specific features of the superstructure formed in charge and orbital ordering, which are caused by substitution of Fe^{3+} for Mn^{3+} ions.

We report here on a study of the temperature dependence of the electrical resistivity and magnetic susceptibility of samples of $La_{1-x}Ca_xMnO_3$ (LCMO) with $x = 0.67$ and $La_{1-x}Ca_xMn_{1-y}Fe_yO_3$ (LCMFO) with $x = 0.67$ and $y = 0.05$ in magnetic fields B ranging from 50 to 10^5 G and in the temperature range $T = 4.2$–400 K. The attention was focused on the irreversible magnetic behavior and electrical conductivity for temperatures $T < T_{CO}$.

2. EXPERIMENT

2.1. Preparation and Characterization of Samples

Ceramic samples of the $La_{1-x}Ca_xMn_{1-y}Fe_yO_3$ ($x = 0.67$, $y = 0.05$) and $La_{1-x}Ca_xMnO_3$ ($x = 0.67$) compounds were prepared by the standard solid-state technology similar to that employed in the synthesis of $La_{1-x}Ca_xMnO_3$ in [18, 19]. A powder of the La_2O_3 oxide is hygroscopic and, therefore, was preliminarily annealed. Mixtures of La_2O_3, $CaCO_3$, MnO_2 and Fe_2O_3 oxide powders were calcined at 1320°C in air for 40 h with intermediate grinding. Then, the powder thus produced was pelletized at 2000 kg/cm^2 and calcined at 1370°C in air for 22 h. The $La_{0.33}Ca_{0.67}MnO_3$ and $La_{0.33}Ca_{0.67}Mn_{0.95}Fe_{0.05}O_3$ samples were characterized by x-ray diffraction [16]. All the samples were single phase and had *Pbnm*-type orthorhombic perovskite structure with the lattice parameters $a \approx b \approx 5.360$ Å, $c \approx 7.609$ Å (LCMO) and $a \approx b \approx 5.364$ Å, $c \approx 7.580$ Å (LCMFO). Doping with iron practically did not affect the lattice parameters.

The chemical composition of a grain in both the iron-doped LCMFO and undoped LCMO samples was very homogeneous. Energy-dispersive x-ray analysis reported in [16] revealed that a change in the composition within a grain expressed in units of the La/Ca ratio was less than 3%. When crossing over from one grain to another, the content of La relative to that of Ca varied from 0.31 to 0.35, with an average of 0.33.

The ratio of the Fe content to the (Mn + Fe) content was equal to a nominal value of 5% in all the grains studied. The grain size was 1–3 μm.

2.2. Magnetic Properties and Electrical Resistivity

The temperature dependence of the magnetic susceptibility $\chi(T)$ of the LCMO and LCMFO samples was investigated with the use of a SQUID magnetometer in the temperature range $T = 4.2$–400 K and magnetic fields of up to 1 T. The sample was cooled from room temperature to 4.2 K in zero field (ZFC) or in a dc field $B = 50$ G or 1 T (FC).

Measurements of the electrical resistivity $\rho(T)$ were conducted by the traditional four-point probe method at temperatures $4.2 < T \le 300$ K upon heating and cooling.

3. RESULTS AND DISCUSSION

3.1. Charge Ordering and Magnetic Behavior

Figure 1 presents the temperature dependence of magnetic susceptibility

$$\chi(T) = \frac{M(T)}{B} \quad (1)$$

for the LCMO and LCMFO samples. Both samples undergo a transition to the charge-ordered state at $T_{CO} = 272 \pm 2$ K and $T_{CO} = 222.0 \pm 2.5$ K, respectively. As the temperature is lowered still more, the LCMO sample reveals a noticeable difference between the susceptibilities χ_{FC} and χ_{ZFC}. At temperatures close to helium temperatures, both samples exhibit differences between the χ_{FC} and χ_{ZFC} curves, which is a manifestation of the so-called irreversible magnetic behavior.

In both (LCMO and LCMFO) samples, the magnetization at high temperatures $T > T_{CO}$ (i.e., above the transition to the charge-ordered state) obeys the Curie–Weiss law

$$\chi(T) = \frac{C}{T - \theta}, \quad (2)$$

where C is the Curie–Weiss constant and θ is the Weiss temperature. The Curie–Weiss constant can be expressed through the effective number p_{eff} of Bohr

magnetons μ_B and the concentration of magnetic ions ($N = 1.74 \times 10^{22}$ cm^{-3} [15])

$$C = p_{\text{eff}}^2 \mu_B^2 \frac{N}{3k}. \quad (3)$$

The fitting parameters for the approximation of the experimental data by the Curie–Weiss law are listed in Table 1. The difference between the theoretical figures (calculated from the mixture rule $p_{\text{eff}}^2 = g^2(S_{Mn^{3+}}(S_{Mn^{3+}} + 1)(1 - x - y) + S_{Mn^{4+}}(S_{Mn^{4+}} + 1)x + S_{Fe}^{3+}(S_{Fe^{3+}} + 1)y)$, where $S_{Mn^{3+}} = 2$, $S_{Mn^{4+}} = 3/2$, $S_{Fe^{3+}} = 5/2$ are the spins of the corresponding magnetic ions) and experimental values of p_{eff} suggests the presence of ferromagnetic clusters. The Weiss temperatures $\theta = 175.8$ K (LCMO) and $\theta = 134.1$ K (LCMFO) assume positive values. Below θ, the ferromagnetic interaction should be dominant. At the same time, the charge and magnetic ordering temperatures for $La_{0.33}Ca_{0.67}MnO_3$ as derived from neutron scattering measurements are $T_{CO} = 270$ K and $T_N = 160$ K (the Néel temperature of the transition to the antiferromagnetic state) [20, 21], thus indicating that the major phase is an antiferromagnetic phase, which implies that the temperature θ should be negative. This contradiction suggests that the compositions under consideration undergo phase separation to produce an antiferromagnetic matrix with embedded ferromagnetic clusters. In the paramagnetic (PM) state at temperatures substantially above T_{CO}, there are no magnetic interactions, the fluctuations are small, and ferromagnetic clusters are not formed. Since the Néel temperature (160 K) for the LCMO sample is lower than the charge-ordering transition temperature, it is conceivable that the magnetic order upon the transition to the charge-ordered state is due to the Coulomb and Jahn–Teller interactions rather than due to the major magnetic interactions (double exchange and superexchange). After the temperature has been lowered, ferromagnetic clusters appear against the paramagnetic background and their presence affects the susceptibility. On the whole, the observed PM–CO transition in the compositions studied reflects the interplay between the ferromagnetic and antiferromagnetic cluster orders.

There are both experimental [22] and theoretical [23] arguments that the perovskite-manganite systems under consideration are capable of forming droplet (cluster) states. Indeed, nonuniform carrier localization gives rise to a nonuniform density of Coulomb energy, which enhances the carrier energy. The system can transfer to an energetically more favorable state through formation of ferromagnetic states, and this is what should bring about formation of ferromagnetic clusters both in the paramagnetic and in the antiferromagnetic matrix.

The dependence $M(B)$ (Figs. 2 and 3) supports the existence of a ferromagnetic component, which grows with decreasing temperature (Fig. 4). This growth is particularly pronounced in the iron-doped sample. Note that the remanent magnetization Δm is very small; indeed, even at 4.2 K, where it is maximum in both compositions, Δm does not exceed 0.3% of theoretical saturation. This evidences a low concentration of ferromagnetic clusters with respect to the antiferromagnetic phase.

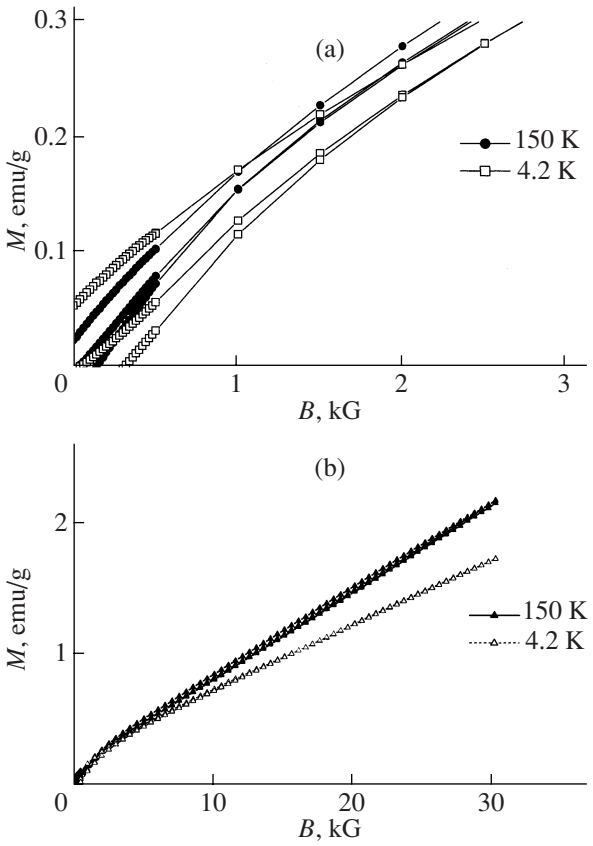

Fig. 2. Dependences of the magnetization on the external magnetic field (hysteresis curves) for LCMO at 4.2 and 150 K: (a) magnetization curve near $B = 0$ on an enlarged scale and (b) general view of the hysteresis curve.

The nonzero values of $(M_{FC} - M_{ZFC})/B$ (Fig. 5) for the LCMO and LCMFO samples suggest that the system is frustrated. A characteristic feature of frustrated

Table 1. Temperatures of the transition to the charge-ordered state and fitting parameters for the approximation of the susceptibility of the paramagnetic phase in the LCMO and LCMFO samples with the Curie–Weiss law

Sample	T_{CO}, K	θ, K	p_{eff}	
			experiment	theory
LCMO	271 ± 2	175.8 ± 1.2	4.83	4.216
LCMFO	222 ± 2.5	134.1 ± 1.1	4.77	4.26

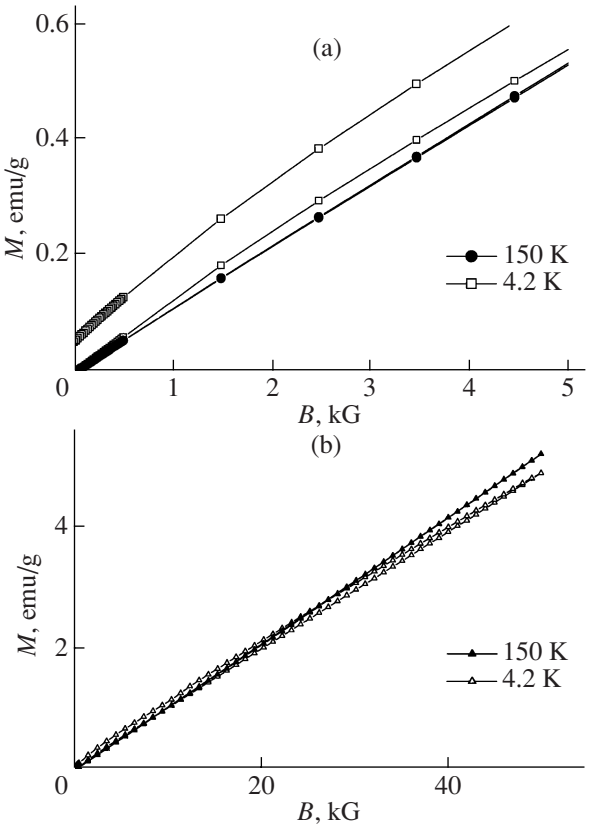

Fig. 3. The same as in Fig. 2 but for LCMFO.

systems is a difference between the FC and ZFC curves (Fig. 1). This difference originates from the spin dynamics and is ordinarily observed below the freezing temperatures of single ions in the spin glass state or freezing temperatures of magnetic cluster moments in cluster spin glass [24]. The frustration effect in the LCMO sample is stronger at temperatures close to T_{CO} ($T < T_{CO}$), i.e., in the range where phase separation has not yet set in and the magnetic susceptibility does not exhibit an irreversible behavior. The charge (orbital) ordering forces formation of the magnetic structure, i.e., favors the interaction between ions or magnetic clusters. In doped compositions, frustration is weaker and Fe^{3+} ions do not create Jahn–Teller distorted octahedra and initiate additional chaos in the stacking of distorted $Mn^{3+}O_6$ octahedra. This additional disorder in the orbital structure reduces the frustration of a system residing in the charge-ordered state. The temperature dependence of $(M_{FC} - M_{ZFC})/B$ displayed in Fig. 5 is very nearly linear in the low-temperature range and weak magnetic fields. The explanation of this dependence may lie in that a decrease in the temperature brings about the growth of the size of the ferromagnetic clusters interacting with one another as magnetic moments do in spin glass [13]. Moreover, the slope of the curve for both samples is the same, with the ordinates differing by a constant value. This implies that iron, rather than being involved in formation of the clusters, only reduces their concentration by its presence. We readily see (Fig. 5) that frustrations in the low-temperature range are less sensitive to the external magnetic field in the case of iron doping, the case where (as we believe) the clusters are of a smaller size and the fraction of the ferromagnetic phase is smaller.

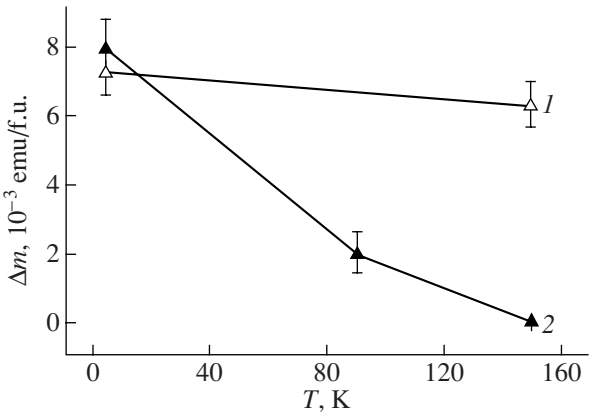

Fig. 4. Dependences of the remanent magnetization Δm on the temperature for the (*1*) LCMO and (*2*) LCMFO samples.

Figure 6 plots the time dependences of the thermoremanent magnetization $M(t)$ of the LCMO and LCMFO samples at $T = 4.2$ K, as well as the magnetization decay rate

$$S(t) = -\frac{dM(t)}{d\log t}. \quad (4)$$

The $S(t)$ graphs for each sample reveal distinct first maxima, which correspond to the relaxation time τ. The

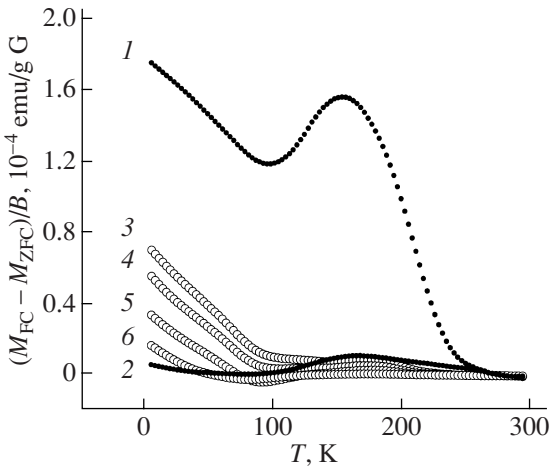

Fig. 5. Temperature dependences of the difference between the susceptibilities $(M_{FC} - M_{ZFC})/B$ for the LCMO (closed symbols) and LCMFO (open symbols) samples at external magnetic fields B = (*1*, *3*) 50 G, (*4*) 150 G, (*5*) 500 G, and (*2*, *6*) 1 T.

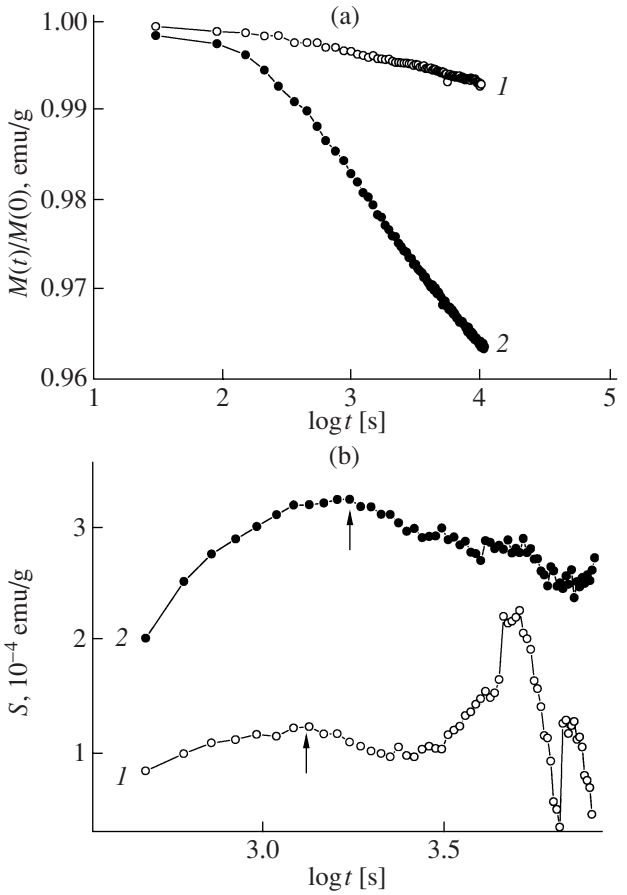

Fig. 6. Time dependences of the (a) thermoremanent magnetization $M(t)/M(0)$ and (b) the rate of magnetization decay $S(t)$ for the (*1*) LCMO and (*2*) LCMFO samples. T = 4.2 K, $H(0)$ = 500 G.

magnetic relaxation (aging) effect is similar to what one observes frequently in substances residing in the spin glass state, and it evidences a specific nonequilibrium state of a frustrated system. The more correlated is the system, the faster the first maximum appears and the more complex is the pattern of the dependence. The more frustrated LCMFO system does not show random magnetization variations and secondary maxima in the decay rate, which suggests a less correlated state of the system. The situation with LCMO is different; indeed, the primary relaxation occurs in a shorter time, and one observes a random oscillation in the $S(t)$ curve, which may evidence more complex correlations in the magnetic spin (or cluster) system in the undoped composition as compared to the composition containing iron.

The evolution of the thermoremanent magnetization can be fitted by a decay law that, to a first approximation, can be described by the relation

$$M(t) = M_0 + M_1 e^{-\left(\frac{t}{\tau}\right)^{1-n}}, \qquad (5)$$

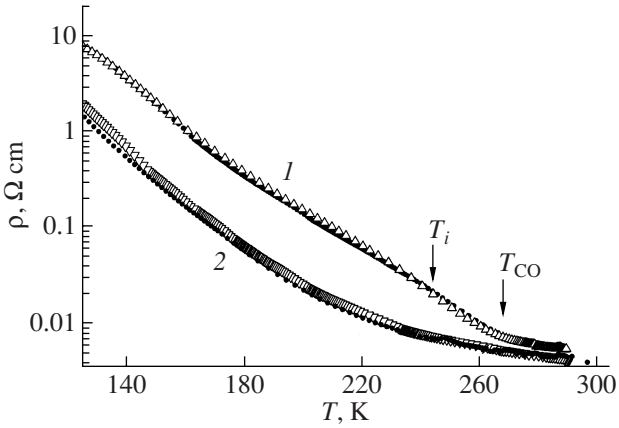

Fig. 7. Temperature dependences of the electrical resistivity $\rho(T)$ of the (*1*) LCMO and (*2*) LCMFO samples upon heating (open symbols) and cooling (closed symbols).

where $n = 0.65 \pm 0.12$ is the fitting parameter [16]. Equation (5) fits better the thermoremanent magnetization data for the LCMFO sample than those for the LCMO sample. The fitting coefficients and characteristic relaxation times are listed in Table 2. Hence, in the low-temperature range, frustrations become manifest more clearly in the iron-containing samples. Iron destroys the ferromagnetic interaction and enhances the frustrations. Besides, Fe^{3+} ions are not involved in the double exchange interaction and strengthen at the corresponding temperatures the spin glass phase.

3.2. Behavior of the Electrical Resistivity

Figure 7 plots the temperature dependences of the electrical resistivity of the LCMO and LCMFO samples. The resistivity of both samples decreases with increasing temperature. The measurements were performed in the cooling and heating modes.

At high temperatures $T > T_{CO}$, the behavior of the electrical resistivity of both compositions under study was analyzed in [16]. It was shown that, in this temperature range, it varies in accordance with the small-radius polaron hopping model [25].

As the temperature decreases, the electrical conductivity may become affected by ever finer interactions (correlations); among them is the Coulomb interaction of charge carriers with one another. The dependence of the electrical resistivity on the temperature (Fig. 7)

Table 2. Fitting parameters for the thermoremanent magnetization decay and relaxation times for the LCMO and LCMFO samples

Sample	M_1, 10^4 emu/g	M_0, 10^{-2} emu/g	τ, 10^3 s
LCMO	4.85 ± 0.11	3.8225 ± 0.0003	1.318 ± 0.057
LCMFO	10.36 ± 0.04	1.4704 ± 0.0002	1.622 ± 0.057

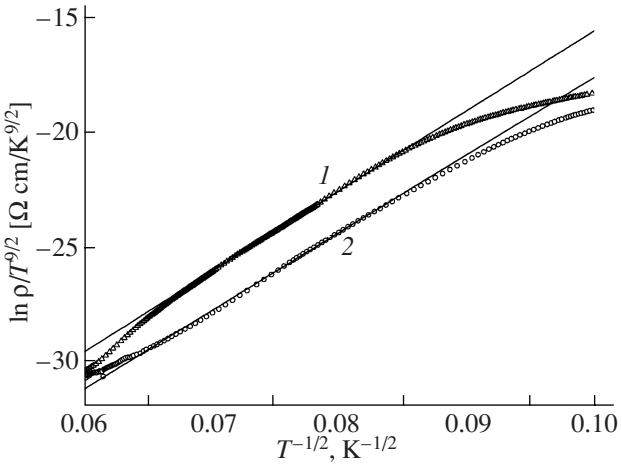

Fig. 8. Temperature dependences of the electrical resistivity in the $T^{-1/2}$–$\ln(\rho/T^{9/2})$ coordinates and their linear approximation upon cooling for the (*1*) LCMO and (*2*) LCMFO samples.

reveals a broad range within which variable-range hopping mechanism operates [26]. The variable-range hopping mechanism described by the Shklovskii–Efros macroscopic law takes into account the Coulomb interaction between charge carriers. This theoretical model permits one to relate macroscopic parameters (the electrical resistivity and its temperature characteristics) with the microscopic parameters of carrier hopping from one localization center to another (the localization radius, characteristic values of the density of states near the Fermi level). We shall use this model to analyze the dependence of the electrical resistivity in order to derive the width of the soft (Coulomb) gap in the density of states in the single-particle model and the relative radius of electron localization (the characteristic parameter of the carrier wave function at hopping centers) [26] from the fitting coefficients.

Figure 8 plots temperature dependences of the electrical resistivity in the $T^{-1/2}$–$\ln\left(\frac{\rho}{T^{9/2}}\right)$ coordinates. The parameters of the hopping conduction mechanism were calculated for the Shklovskii–Efros model

$$\rho(T) = \rho_0(T)\exp\left(\left(\frac{T_0}{T}\right)^p\right), \quad (6)$$

where the preexponential factor depends on temperature

$$\rho_0(T) = AT^m, \quad (7)$$

T_0 is the characteristic Shklovskii–Efros temperature, $p = 1/2$, $m = 9/2$ [15], and A is the preexponential factor in the Shklovskii–Efros law. The electrical resistivities of both LCMO and LCMFO samples follow relation (6) in the range 150–200 K. The highest temperature at which Eq. (6) is still valid is called the activation temperature T_v of variable-range hopping conduction. This temperature makes it possible to calculate the width of the soft Coulomb gap [15] in the density of states of the single-particle model from the relation

$$\Delta = k\sqrt{T_0 T_v}. \quad (8)$$

The characteristic parameters of this temperature dependence are presented in Table 3. The microparameter Δ (the Coulomb gap width) can be estimated from the expression for the electrostatic interaction energy

$$\Delta = \frac{e^2}{4\pi\kappa\varepsilon_0 r}, \quad (9)$$

$$r = 2\left(\frac{4}{3}\pi N\right)^{-\frac{1}{3}}, \quad (10)$$

$$N = N_0(1 - x - y), \quad (11)$$

where e is the elementary charge, ε_0 is the dielectric constant, κ is the effective permittivity, r is the average distance between Mn^{3+} ions, $N_0 = 1.74 \times 10^{22}$ cm^{-3} is the manganese ion concentration [15], and x and y are the Ca and Fe concentrations ($x = 0.67$; $y = 0, 0.05$). The Coulomb interaction energies for the undoped and Fe-doped materials were 0.569 and 0.538 eV, respectively. The concentration of localized electrons, just as that of Mn^{3+} ions, decreases as the latter ions are substituted by Fe^{3+} ions, provided the e_g iron electrons remain localized. The soft gap parameters derived from the fitting microparameters for the experimental curves were found to be 0.464 and 0.446 for the compositions with $y = 0$ and 0.05, respectively. They agree with the estimates and substantiate the suggestion that the e_g electrons of Fe^{3+} ions are not involved in the transport processes in the temperature range under consideration.

Table 3. Fitting and characteristic parameters used for approximating the temperature dependence of the electrical resistivity with the variable-range hopping model

Sample	Mode	$A \times 10^{-20}$, Ω cm K$^{-9/2}$	T_0, K	T_v, K	Λ, eV	a/a_{und}	T_i(infl), K
LCMO	$T\downarrow$	0.00459 ± 0.00009	131276 ± 220	220.5 ± 0.9	0.4640 ± 0.0014	0.880	245.3
	$T\uparrow$	0.0132 ± 0.0009	122010 ± 680	210 ± 3	0.436 ± 0.004		239
LCMFO	$T\downarrow$	0.00105 ± 0.00009	128271 ± 800	208 ± 2	0.446 ± 0.003		–
	$T\uparrow$	0.0006 ± 0.0001	134066 ± 1900	178.1 ± 0.5	0.421 ± 0.004		–

The microparameters thus obtained (A is the preexponential factor in Eq. (7), T_0 is the characteristic temperature, and T_v is the activation temperature of variable-range hopping, which is the highest temperature at which Eq. (6) is still valid, and, hence, the lowest on the $T^{-1/2}$ scale) yield the relative localization radius a (one of the parameters in the percolation model [26]). The relation [15]

$$A = \left(\frac{C}{2^q}\right) a^{11} T_0^{(7+q)p} \tag{12}$$

permits one to estimate the ratio of the localization radii for the samples under study (C is a constant). Based on the light iron doping and the closeness in magnitude between the ionic radii of Fe and Mn, it was assumed that the C constants of the two compositions are comparable. The q and p parameters in Eq. (12) are 0 and 1/2, respectively; they were adopted from the problem of variable-range hopping conduction including Coulomb interaction (the Shklovskii–Efros mechanisms) under the assumption of a hydrogen-like electron wave function [15]. The ratio of the localization radii for the iron-doped and undoped samples is 0.88. This suggests that the iron doping enhances the degree of carrier localization. In this case, the probability for an electron to hop from one localization center to another is lower. The electric resistivity of the LCMFO sample is, however, lower than that of the LCMO sample. This may be attributed to the fact that the doping with iron destroys orbital (and, hence, stripe) order of the charge-ordered state to a larger extent than it increases carrier localization. Orbital ordering induces antiferromagnetic ordering, thus enhancing the electrical resistivity [2]. At high iron concentrations, however, the two mechanisms may produce comparable effects, and the resistivity of the material will start to grow.

Thus, the behavior of electrical resistivity in the samples under study depends, in many respects, on the charge (orbital) ordering and the doping with iron initiates additional disorder into the charge (orbital) and magnetic structures.

As follows from an analysis of the dependence of the electrical resistivity on the temperature (Fig. 7), in the vicinity of the charge-ordering transition, one observes a shoulder, which is particularly noticeable for the undoped composition. It occurs at the temperature T_i satisfying the relation

$$\left.\frac{d\log\rho(T)}{dT}\right|_{T=T_i} = \min. \tag{13}$$

The phase transition to the charge-ordered (orbitally ordered) state induces antiferromagnetic order and charge nonuniformity [2]. This is most clearly seen in the LCMO sample, whose temperature dependence exhibits a distinct shoulder (245.3 K) near the charge-ordering temperature, which we determined from magnetic measurements.

4. CONCLUSIONS

We have studied the effect of iron doping on the electron-doped perovskite manganites. We have performed studies of the magnetic susceptibility, magnetization, magnetic relaxation, and electrical resistivity of $La_{1-x}Ca_xMn_{1-y}Fe_yO_3$ samples ($x = 0.67$, $y = 0$ and $x = 0.67$ and $y = 0.05$). The results obtained suggest that these compositions exhibit charge (orbital) ordering, as well as phase separation. Below the temperature of the transition to the charge-ordered state, magnetic order sets in through correlation with orbital ordering, which, in turn, is initiated by the so-called Jahn–Teller vibronic interaction [2]. The orbital ordering is conducive to the frustration, which is most clearly pronounced in the undoped composition. While the Fe-doped composition also exhibits charge (orbital) ordering, frustrations manifest themselves to a lesser extent because of the Mn^{4+}–Fe^{3+} ion pairs not being involved in the double exchange interaction. Studies of the magnetization revealed the presence of a ferromagnetic component in both samples. The remanent magnetization of the doped sample is much lower in the temperature range 100–200 K, which evidences the disordering part played by iron and suggests that iron ions are not involved in the double exchange interaction. As the temperature is lowered still more, the remanent magnetizations of the undoped and doped samples become equal to each other. The studies of thermoremanent magnetization relaxation, combined with the data obtained on the magnetic susceptibility, permit the conclusion that, in the low-temperature range, the LCMO and LCMFO compositions are in the cluster spin-glass state. The specific features observed in the behavior of LCMFO relaxation give grounds to assume that clusters in LCMFO are of a smaller characteristic size than those in LCMO. An analysis of the data on the electrical resistivity showed that the formation of the charge-ordered phase (particularly in LCMO) increases somewhat the electrical resistivity (particularly in LCMO) as a result of the formation of the weakly conducting antiferromagnetic phase. The growth of the electrical resistivity in the LCMFO sample is accompanied by an increase in the degree of charge carrier localization. For the iron doping level and carrier concentrations realized in the samples, the formation of the charge-ordered state affects the magnetic properties and the electrical resistivity of the LCMFO sample stronger than the charge carrier localization does.

ACKNOWLEDGMENTS

This study was supported by the Wihuri Foundation (Finland) and the Belgorod State University (project no. VKG 005-07).

REFERENCES

1. V. M. Loktev and Yu. G. Pogorelov, Fiz. Nizk. Temp. (Kharkov) **26** (3), 231 (2000) [Low Temp. Phys **26** (3), 171 (2000)].
2. J. M. D. Coey, M. Viret, and S. von Molnar, Adv. Phys. **48**, 167 (1999).
3. M. Roy, F. J. Mithel, A. P. Ramirez, and P. E. Shiffer, J. Phys.: Condens. Matter **11**, 4834 (1999).
4. P. Levy, F. Parisi, G. Polla, D. Vega, G. Leyva, H. Lanza, R. S. Freitas, and L. Ghivelder, Phys. Rev. B: Condens. Matter **62**, 6437 (2000).
5. A. Moreo, S. Yukoni, and E. Dagoto, Science (Washington) **283**, 2034 (1999).
6. Y. Morimoto, A. Mashida, S. Mori, N. Yamamoto, and A. Nakamura, Phys. Rev. B: Condens. Matter **60**, 9220 (1999).
7. K. H. Ahn, X. W. Wu, K. Liu, and C. L. Chein, Phys. Rev. B: Condens. Matter **54**, 15299 (1996).
8. X. Chen, Z. Wang, R. Li, B. Shen, W. Zhan, J. Sun, J. Chen, and Ch. Yan, J. Appl. Phys. **87**, 5594 (2000).
9. R. Laiho, K. G. Lisunov, E. Lähderanta, V. N. Stamov, V. S. Zakhvalinskii, A. I. Kurbakov, and A. E. Sokolov, J. Phys.: Condens. Matter **16**, 881 (2004).
10. A. Simopoulus, M. Pissas, G. Kallias, E. Devlin, N. Moutis, I. Panagiotopoulos, D. Niarchos, C. Christides, and R. Sonntag, Phys. Rev. B: Condens. Matter **59**, 1263 (1999).
11. M. Pissas, G. Kallias, E. Devlin, A. Simopoulus, and D. Niarchos, J. Appl. Phys. **81**, 5770 (1997).
12. R. D. Shannon, Acta Crystallogr., Sect. A: Cryst. Phys., Diffr., Theor. Gen. Crystallogr. **32**, 751 (1976).
13. R. Laiho, K. G. Lisunov, E. Lähderanta, J. Salminen, V. N. Stamov, and V. S. Zakhvalinskii, J. Magn. Magn. Mater. **250**, 267 (2002).
14. R. Laiho, K. G. Lisunov, E. Lähderanta, J. Salminen, M. A. Shakhov, V. S. Stamov, P. A. Petrenko, and V. S. Zakhvalinskii, J. Phys. Chem. Solids **64**, 1573 (2003).
15. R. Laiho, K. G. Lisunov, E. Lähderanta, P. A. Petrenko, J. Salminen, M. A. Shakhov, M. O. Safontchik, V. N. Stamov, M. L. Shubnikov, and V. S. Zakhvalinskii, J. Phys.: Condens. Matter **14**, 8043 (2002).
16. T. S. Orlova, J. Y. Laval, P. Monod, J. G. Noudem, V. S. Zahvalinskii, V. S. Vikhnin, and Yu. P. Stepanov, J. Phys.: Condens. Matter **18**, 6729 (2006).
17. T. S. Orlova, J.-Y. Laval, V. S. Zakhvalinskiĭ, and Yu. P. Stepanov, Fiz. Tverd. Tela (St. Petersburg) **48** (11), 1994 (2006) [Phys. Solid State **48** (11), 2115 (2006)].
18. R. Laiho, K. G. Lisunov, E. Lähderanta, P. A. Petrenko, J. Salminen, V. N. Stamov, and V. S. Zakhvalinskii, J. Phys.: Condens. Matter **12**, 5751 (2000).
19. R. Laiho, K. G. Lisunov, E. Lähderanta, P. A. Petrenko, V. N. Stamov, and V. S. Zakhvalinskii, J. Magn. Magn. Mater. **213**, 271 (2000).
20. P. Schiffer, A. Ramirez, W. Bao, and S. W. Cheong, Phys. Rev. Lett. **75**, 3336 (1995).
21. M. R. Ibarra, J. M. de Teresa, J. Blasco, P. A. Algarabel, C. Marquina, J. Garcia, J. Stankiewicz, and C. Ritter, Phys. Rev. B: Condens. Matter **56**, 8252 (1997).
22. G. Allodi, R. de Renzi, G. Guidi, F. Licci, and M. W. Pieper, Phys. Rev. B: Condens. Matter **56**, 6036 (1997).
23. M. Yu. Kagan and K. I. Kugel', Usp. Fiz. Nauk **171** (6), 577 (2001) [Phys. Usp. **44** (6), 553 (2001)].
24. R. Laiho, K. G. Lisunov, E. Lähderanta, V. S. Zakhvalinskii, V. L. Kozhevnikov, I. A. Leonidov, E. B. Mitberg, and M. V. Patrakeev, J. Magn. Magn. Mater. **293**, 892 (2005).
25. M. Jaime, M. B. Salomon, M. Rubinstein, R. E. Treece, J. S. Horwitz, and D. B. Chrisey, Phys. Rev. B: Condens. Matter **54**, 11914 (1996).
26. B. I. Shklovskii and A. L. Efros, *Electronic Properties of Doped Semiconductors* (Springer, Berlin, 1984).

Translated by G. Skrebtsov